


Temperature-induced iron oxidation in bafertisite $\text{Ba}_2\text{Fe}_4^{2+}\text{Ti}_2(\text{Si}_2\text{O}_7)_2\text{O}_2(\text{OH})_2\text{F}_2$: X-ray diffraction and Mössbauer spectroscopy study

Elena S. Zhitova^{1,2}  · Andrey A. Zolotarev¹ · Sergey V. Krivovichev^{1,3} · Alexey G. Goncharov¹ · Faina A. Gabdrakhmanova¹ · Nikolay V. Vladykin⁴ · Maria G. Krzhizhanovskaya¹ · Vladimir V. Shilovskikh⁵ · Natalia S. Vlasenko⁵ · Anatoly A. Zolotarev¹

Published online: 21 November 2017

© Springer International Publishing AG, part of Springer Nature 2017

Abstract The high-temperature behavior of bafertisite was studied by combination of techniques in order to characterize the temperature-induced iron oxidation associated with deprotonation of an octahedral layer. The chemical formula of bafertisite from Darai-Pioz alkaline complex (Tajikistan) determined by electron-microprobe analyzes and Mössbauer spectroscopy is $\text{Ba}_{2.11}(\text{Fe}_{2.70}^{2+}\text{Fe}_{0.17}^{3+}\text{Mn}_{1.09}\text{Zr}_{0.04}\text{Na}_{0.03})(\text{Ti}_{1.96}\text{Nb}_{0.07})(\text{Si}_2\text{O}_7)_2\text{O}_2(\text{OH})_{1.29}\text{O}_{0.65}\text{F}_{0.06}\text{F}_2$. *In situ* high-temperature powder X-ray diffraction revealed abrupt shift of

This article is part of the Topical Collection on *Proceedings of the International Conference on the Applications of the Mössbauer Effect (ICAME 2017), Saint-Petersburg, Russia, 3–8 September 2017* Edited by Valentin Semenov

Electronic supplementary material The online version of this article (<https://doi.org/10.1007/s10751-017-1468-9>) contains supplementary material, which is available to authorized users.

✉ Elena S. Zhitova
zhitova_es@mail.ru

¹ Institute of Earth Sciences, St. Petersburg State University, University Emb. 7/9, Saint-Petersburg 199034, Russia

² Institute of Volcanology and Seismology, Russian Academy of Sciences, Piip blvd. 9, Petropavlovsk-Kamchatsky 683006, Russia

³ Nanomaterials Research Center, Kola Science Center, Russian Academy of Sciences, Fersmana Str. 14, Apatity 184209, Russia

⁴ Vinogradov Institute of Geochemistry, Siberian Branch, Russian Academy of Sciences, Favorskogo str., 1a, Irkutsk 664033, Russia

⁵ Resource Center, St. Petersburg State University, Universitetskaya nab. 7/9, St. Petersburg 199034, Russia

reflections to the high-angle region and reduction of their intensity at $T > 525$ °C. The Mössbauer spectroscopy studies indicated that the crystal structure of bafertisite contains Fe in octahedral sites as predominantly ferric ions with $\text{Fe}^{3+}/\Sigma\text{Fe} = 0.06$, whereas bafertisite annealed at $T = 600$ °C has Fe in the same position with $\text{Fe}^{3+}/\Sigma\text{Fe}$ up to 0.39. The differential scanning calorimetry and thermogravimetric analyzes reveal the occurrence of a broad exothermic effect at $T \sim 537$ °C associated with the mass loss corresponding to deprotonation. Since in the studied sample of bafertisite, Fe^{2+} *apfu* strongly prevails over OH *apfu*, the stoichiometric (charged-balanced) high-temperature oxidized modification cannot be obtained. In the paper, the high-temperature behavior of bafertisite is discussed and compared to that of astrophyllite.

Keywords Bafertisite · Iron oxidation · High-temperature crystal chemistry · Deprotonation · Layered titanosilicates

1 Introduction

Bafertisite, ideally $\text{Ba}_2\text{Fe}_4^{2+}\text{Ti}_2(\text{Si}_2\text{O}_7)_2\text{O}_2(\text{OH})_2\text{F}_2$, belongs to the large family of layered titanosilicates [1, 2]. The crystal structure of bafertisite contain complex layers consisting of octahedral sheets (*O*) formed by MO_6 octahedra ($M = \text{Fe}, \text{Mn},$ and minor Zr, Na) and sandwiched between two heteropolyhedral sheets (*H*) formed by Si_2O_7 groups linked by TiO_6 octahedra with the Ti:Si ratio equal to 1:2 (Fig. 1). In the crystal structure, the *HOH* blocks [or TS (titanosilicate) blocks] are connected *via* interlayer Ba^{2+} cations [3]. Bafertisite was first described as a widespread hydrothermal mineral in the iron deposit Baiyun-Obo, China [4] and since then was reported from Gremyakha-Vyrmes (Kola peninsula, Russia) [3, 5] and Darai-Pioz (Tajikistan) alkaline complexes [3]. The crystal structure solution and refinement of the mineral was done by several groups of researchers [3, 6, 8, 9].

Along with other 44 structurally and chemically similar species, bafertisite belongs to the seidozerite supergroup of minerals [10]. From the crystal chemical point of view, minerals of this supergroup or layered (*HOH*) titanosilicates have strong resemblance to the phyllosilicates of the mica supergroup (see [7, 11] for more details) as both are based upon mixed octahedral-tetrahedral layers. In the context of the current study, this similarity is essential, because Fe-containing minerals from both groups experience temperature-induced iron oxidation coupled with deprotonation reactions (as observed for Fe-rich phlogopite [12–15], illite [16], biotite [17] and vermiculite [18]).

The temperature-induced iron oxidation was recently reported for astrophyllite, ideally $\text{K}_2\text{NaFe}_7^{2+}\text{Ti}_2(\text{Si}_4\text{O}_{12})_2\text{O}_2(\text{OH})_4\text{F}$ [19]. The crystal structures of astrophyllite and bafertisite are related and consist of the *HOH* blocks with alkali and alkali-earth cations in the interlayer. At the same time, the two structures are different in the linkage of adjacent *HOH* blocks. In bafertisite, the *HOH* blocks are separated by the layers of Ba atoms [3], whereas, in astrophyllite, adjacent *HOH* blocks are connected *via* corner sharing of two $\text{Ti}\varphi_6$ ($\varphi = \text{F}, \text{OH}, \text{O}$) octahedra, i.e. formation of the Ti- φ -Ti linkage along the direction of layer stacking [20, 21]. In addition, bafertisite and astrophyllite are different in the topology of the octahedral layers (Fig. 1b, c). However, both astrophyllite and bafertisite have: (i) Fe^{2+} as prevalent cations within octahedral layers and (ii) protonated oxygen atoms inside the octahedral layers. These two features point out that bafertisite, by analogy with astrophyllite, may experience a temperature-induced iron oxidation, which initiated the current study that was carried out by the combination of X-ray diffraction analysis and Mössbauer spectroscopy.

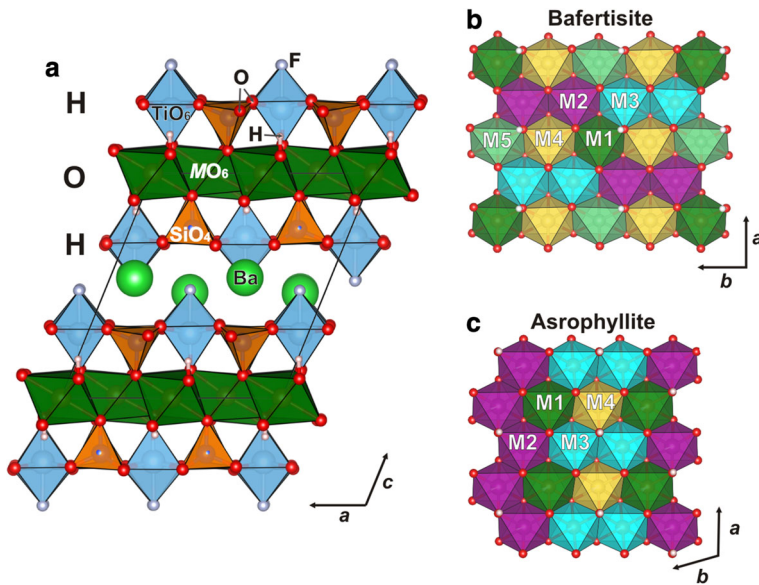


Fig. 1 **a** The crystal structure of bafertisite, with two *HOH* blocks separated by the layer of Ba atoms; **b** topology of the octahedral (*O*) layer in bafertisite and **c** topology of the octahedral layer in astrophyllite

2 Materials and methods

2.1 Materials

The bafertisite sample (indicated herewith as BaFeTi25) studied in this work originate from the Darai-Pioz alkaline complex, Tajikistan. In order to characterize its high-temperature modification, the sample was kept in an oven under the following regime: 30 min heating from 25 to 600 °C, keeping at 600 °C for 60 min., followed by cooling to the room temperature. The annealed sample is hereafter denoted as BaFeTi600.

2.2 Electron microprobe analysis

Several crystals of bafertisite were mounted in epoxy blocks, polished and carbon-coated. The chemical composition of bafertisite was determined with a scanning electron microscope Hitachi S3400N equipped with INCA Wave 500 wavelength-dispersive spectrometer. Operating conditions were as follows: acceleration voltage 20 kV, probe current 10 nA, peak and background acquisition were 30 s and 15 s, respectively. The results and other details are given in Table 1.

2.3 High-temperature powder X-ray diffraction

Thermal behavior of bafertisite was studied by *in situ* high-temperature X-ray diffraction in the 25–1000 °C temperature range in air by means of the Rigaku Ultima IV powder X-ray diffractometer (CuK α_{1+2} radiation, 40 kV/30 mA, Bragg–Brentano geometry, PSD D-Tex Ultra) equipped with the Rigaku HT 1500 high-temperature attachment. A thin powder

Table 1 The chemical composition of bafertisite

Constituent (wt. %)	BaFeTi25	BaFeTi600	Standard	Constituent (<i>apfu</i>)	BaFeTi25	BaFeTi600
BaO	29.90		BaF ₂	Ba	2.11	
				Σ	2.11	
FeO ¹	17.89	11.61	FeS ₂	Fe ²⁺	2.70	1.75
Fe ₂ O ₃ ¹	1.27	8.25	FeS ₂	Fe ³⁺	0.17	1.12
MnO	7.11		Mn	Mn	1.09	
Na ₂ O	0.10		NaCl	Na	0.03	
ZrO ₂	0.36		Zr	Zr	0.04	
				Σ	4.03	
TiO ₂	14.43		Ti	Ti	1.96	
Nb ₂ O ₅	0.82		Nb	Nb	0.07	
				Σ	2.03	
SiO ₂	23.65		SiO ₂	Si	4.00	
				Σ	4.00	
F	3.61		BaF ₂	F	2.06	
H ₂ O ²	1.07	0.28		OH	1.29	0.34
F=O	1.52					
Total	98.70	98.60				

1 – calculated based on the Mössbauer spectroscopy data;

2 – calculated on the basis of charge balance

sample was deposited on a Pt sample holder ($20 \times 12 \times 2 \text{ mm}^3$) from a heptane suspension. The temperature step and the heating rate were 25°C and $4^\circ / \text{min}$, respectively.

The unit-cell parameters of bafertisite at different temperatures were refined by the Rietveld method by means of Topas 4.2 [22] using the structural model that is triclinic, space group *C*-1 [3]. The Rietveld refinement was performed starting from cell and atom coordinates of bafertisite from Darai-Pioz Glacier taken from Cámara et al. [3] with the atom coordinates, site scattering and isotropic-displacement parameters fixed during refinement. Neutral scattering factors were used for all atoms. The background was modeled using a Chebychev polynomial approximation of the 20th order. The peak profile was described using the fundamental parameters approach. Zero shift was refined at every step. Refinement of preferred orientation parameters confirmed the presence of a significant preferred orientation along the [001] direction. The results of structure refinements at different temperatures are given in the Online Resource 1. The unit-cell parameters can be refined only in the temperature range $25\text{--}525^\circ \text{C}$, due to the significant decrease in intensity after 525°C (Fig. 2). In the temperature range $550\text{--}700^\circ \text{C}$ only d_{002} -values could be determined.

2.4 Mössbauer spectroscopy

Mössbauer spectra for bafertisite (BaFeTi25) and its high-temperature modification (BaFeTi600) were collected using SM-1201 spectrometer at room temperature in a constant acceleration mode over a velocity range of $\pm 7 \text{ mm/s}$ with a nominal $50 \text{ mCi } ^{57}\text{Co}$ source in a Rh matrix with 10 hours counting time. The spectrometer was calibrated relative to metallic iron at room temperature. Powdered absorbers were pressed in plastic disks and fixed on

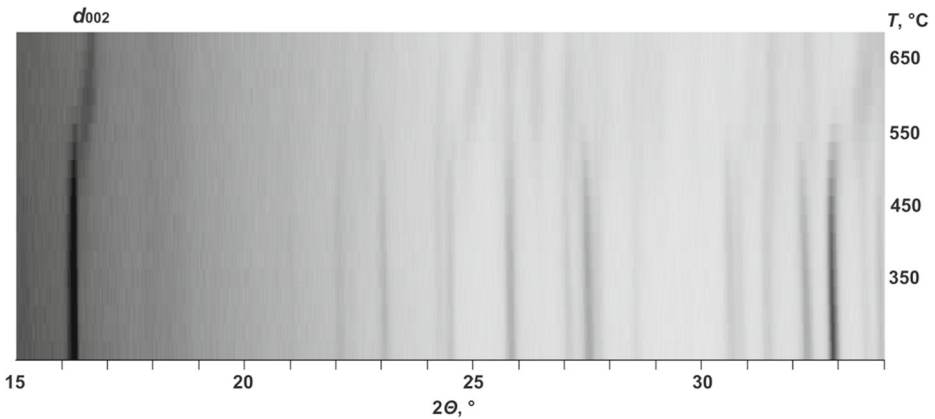


Fig. 2 The evolution of powder X-ray diffraction pattern of bafertsite with temperature

a special aluminum holder to avoid preferred orientation of mineral grains. The density of the natural iron in the absorber was $<5 \text{ mg/cm}^2$. The spectra were approximated by a sum of Lorentzian lines using the MOSSFIT©software. The relative amounts of Fe^{2+} and Fe^{3+} and their site positions in the crystal lattice were determined from integral doublet intensities and hyperfine parameters, assuming equal Mössbauer effect probabilities for Fe^{2+} and Fe^{3+} at different sites.

2.5 Differential scanning calorimetry (DSC) and thermogravimetric analysis (TG)

Differential scanning calorimetry (DSC) and thermogravimetric analysis (TG) were done using a DSC/TG Netzsch STA 449 F3 instrument in the 30–1000 °C temperature range at the ramp rate of 10 °C min^{-1} , gas flow 20 ml/min by heating the samples under Ar–O atmosphere.

3 Results

3.1 Chemical composition

The averaged electron-microprobe data are given in Table 1. The chemical formula was obtained by the combination of electron-microprobe analyzes and Mössbauer spectroscopy and calculated on the basis of $\text{Si} = 4$. The chemical formula of bafertsite (BaFeTi_{25}) and its HT modification (BaFeTi_{600}) are $\text{Ba}_{2.11}(\text{Fe}_{2.70}^{2+}\text{Fe}_{0.17}^{3+}\text{Mn}_{1.09}\text{Zr}_{0.04}\text{Na}_{0.03})(\text{Ti}_{1.96}\text{Nb}_{0.07})(\text{Si}_2\text{O}_7)_2\text{O}_2(\text{OH}_{1.29}\text{O}_{0.65}\text{F}_{0.06})\text{F}_2$ and $\text{Ba}_{2.11}(\text{Fe}_{1.75}^{2+}\text{Fe}_{1.12}^{3+}\text{Mn}_{1.09}\text{Zr}_{0.04}\text{Na}_{0.03})(\text{Ti}_{1.96}\text{Nb}_{0.07})(\text{Si}_2\text{O}_7)_2\text{O}_2(\text{OH}_{0.34}\text{O}_{1.60}\text{F}_{0.06})\text{F}_2$, respectively, with the main difference being in the Fe oxidation state and the OH/O ratio.

3.2 X-ray diffraction

The unit-cell parameters refined from the powder pattern recorded at room temperature are $a = 10.6820(7)$, $b = 13.7656(9)$, $c = 11.7402(8)$ Å, $\alpha = 90.355(5)$, $\beta = 112.233(5)$, $\gamma =$

$89.989(6)^\circ$, $V = 1598.0(2) \text{ \AA}^3$ close to that reported recently [3]. The evolution of unit-cell parameters *versus* temperature shows the expansion of the crystal structure of bafertisite in the temperature range 25–450 °C. The unit-cell parameters refined at $T = 475, 500$ and 525 °C indicated the changes in the thermal behavior of bafertisite after 450 °C (Fig. 3). The main coefficients of the thermal-expansion tensor were determined using a second-order approximation of temperature dependencies for the unit-cell parameters in the range 25–450 °C by the DTC program [23, 24]. The thermal-expansion tensor was visualized using the TEV program [25].

3.3 Mössbauer spectroscopy

The Mössbauer spectra for bafertisite (BaFeTi25) and its high-temperature modification (BaFeTi600) are shown in Fig. 4. Selected hyperfine parameters are given in Table 3. The spectrum for the room-temperature sample shows absorptions peaks due to both Fe^{2+} (QS = 2.00(2) mm/s and IS = 1.13(1) mm/s) and Fe^{3+} (QS = 0.92(5) mm/s and IS = 0.58(3) mm/s) in octahedral positions with mostly ferric state of iron ($\text{Fe}^{3+}/\Sigma\text{Fe} = 0.06$). These results are in good agreement with Semenov et al. [4], whereas in other studies Fe was found exclusively in ferric state [3, 26, 27]. The high-temperature sample shows Fe in the same position (QS = 2.02(2) and 1.05(5), IS = 1.13(1) and 0.50(4), for Fe^{2+} and Fe^{3+} respectively), but with the $\text{Fe}^{3+}/\Sigma\text{Fe}$ ratio of up to 0.39. The full widths at half maximum (FWHM) of the lines increase slightly for the Fe^{2+} peak and twice for Fe^{3+} component for high-temperature sample, possibly showing stress in a structure that is collapsing (see below).

3.4 DCS/TG

The DSC and TG curves are shown in Fig. 5. The first effect occurs at $T = 316$ °C with the mass loss of 2.73%. This effect was not manifested by the dependencies of unit-cell parameters (Fig. 5) and difficult to interpret. The second effect is found around 537 °C and corresponds to the iron oxidation. The associated mass loss agrees with deprotonation. The effects observed at temperature above 800 °C are due to the decomposition of the mineral.

4 Discussion

4.1 General features of high-temperature behavior of bafertisite

Bafertisite experiences temperature-induced iron oxidation coupled with deprotonation registered at temperature above 450 °C. The iron oxidation is manifested by: (i) the change in the thermal behavior of bafertisite after 450 °C (Fig. 3) and (ii) the presence of the broad exothermic effect associated with the mass loss corresponding to deprotonation at ~ 537 °C (Fig. 5). The iron oxidation is unambiguously confirmed by the Mössbauer spectroscopy (Fig. 4), which indicated oxidation of 33% of Fe^{2+} after annealing at 600 °C. At temperatures above 525 °C the high-temperature oxidized modification is characterized by the simultaneous decrease in the intensity of diffraction maxima and the shift of some reflections (including d_{002} plotted at Fig. 3) toward the high-angle region (Fig. 2). Due to the significant reduction of intensity, it was impossible to use single-crystal XRD, which could potentially provide more details on the structural deformations. In general, bafertisite is characterized by a damping volume expansion with the increase of temperature (Table 2).

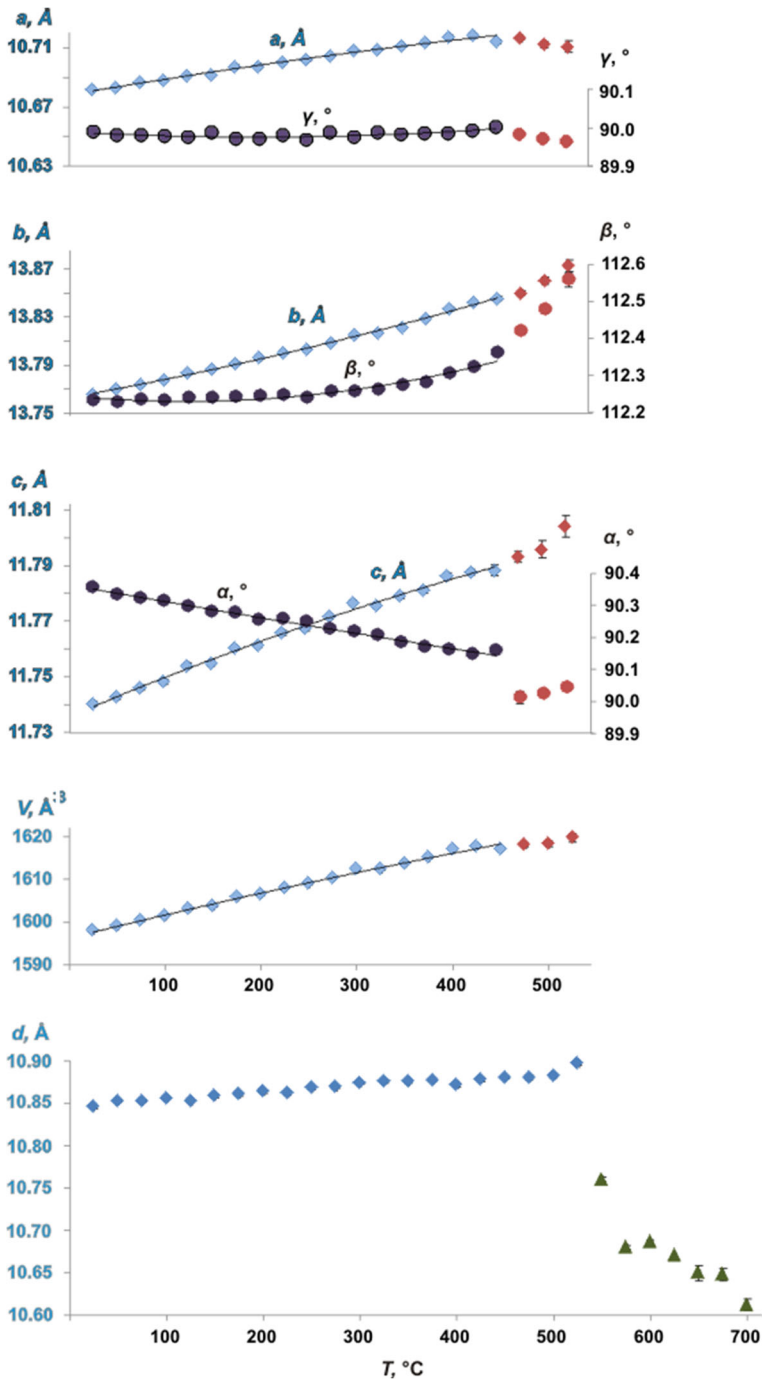


Fig. 3 The evolution of the unit-cell parameters and d_{002} -value of bafertsite with the increasing temperature (the errors of calculation is mainly within the bars). The last three symbols at each graph (red) correspond to partially oxidized modification of bafertsite

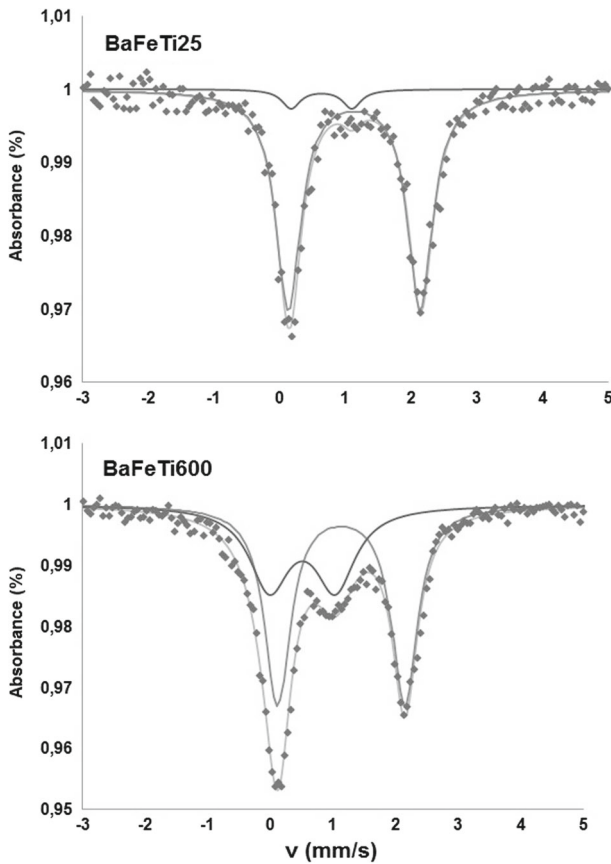


Fig. 4 The Mössbauer spectra of bafertisite (BaFeTi25) and its high-temperature modification (BaFeTi600)

By analyzing the coefficient of thermal expansion along eigenvectors and crystallographic axes (Table 2), it can be concluded that the expansion along α_{22} and α_{33} goes at the same rate when temperature increases (Table 2), whereas the expansion along α_{11} (Fig. 6b) at 100 °C ($6.6 \text{ }^\circ\text{C}^{-1}$) is replaced by contraction at 500 °C ($-3.4 \text{ }^\circ\text{C}^{-1}$). Most likely, this effect indicates the reduction of thickness of the octahedral layer (t_{oct}) due to the shortening of Fe-O interatomic distances and flattening of MO_6 octahedra due to the iron oxidation [19]. The same is outlined by reduction of the d -value (Fig. 3). Regarding anisotropy of thermal expansion ($\alpha_{\text{max}}/\alpha_{\text{min}}$) of bafertisite, it increases from 1.2 ($T = 100 \text{ }^\circ\text{C}$) to 2.8 ($T = 500 \text{ }^\circ\text{C}$) due to decrease of α_{11} as mentioned above (Table 2).

4.2 Comparison to previous data

When compared to astrophyllite [19], the high-temperature behavior of bafertisite is similar in general features: (i) the temperature of iron oxidation (450 °C for bafertisite and 500 °C for astrophyllite); (ii) abrupt shift of some reflections to the high-angle region in the powder XRD pattern; (iii) broad exothermic effect (537 °C for bafertisite and 584

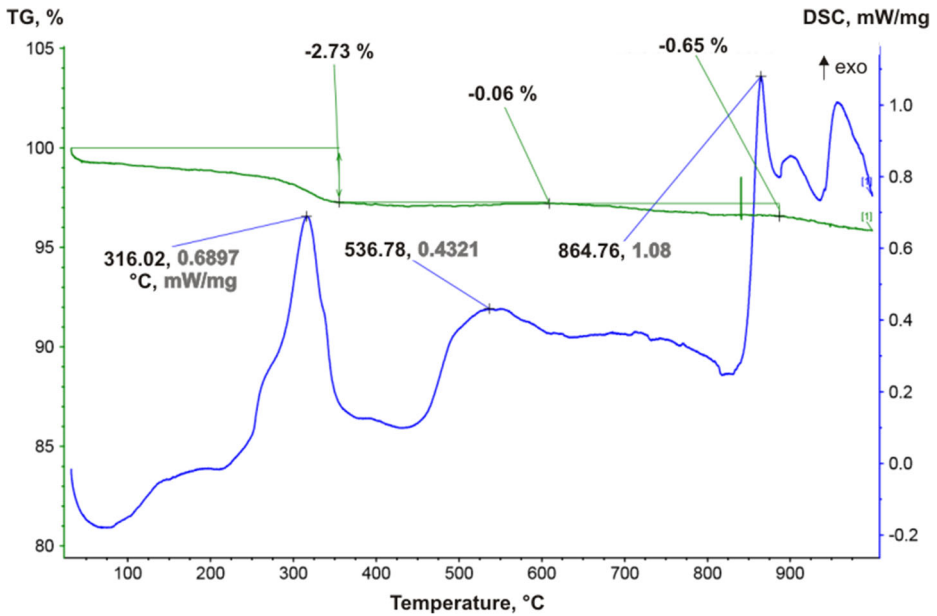


Fig. 5 DTA and TG curves of bafertsite

Table 2 Thermal expansion/contraction coefficients ($10^{-6}, ^\circ\text{C}^{-1}$) of bafertsite compared to astrophyllite

	Bafertsite					Astrophyllite ¹
$T, ^\circ\text{C}$	100	200	300	400	500	300
α_{11}	6.6	5.5	3.0	-0.1	-3.4	-0.8
α_{22}	16.7	16.3	16.8	17.7	18.9	10.5
α_{33}	9.5	9.1	9.2	9.4	9.7	6.7
μ_{a1}^2	81.5	64.2	56.3	54.5	54.2	30.6
μ_{b2}^2	45.4	36.0	30.6	27.4	25.2	65.4
μ_{c3}^2	59.5	52.7	46.5	43.1	41.0	44.9
α_a	9.4(7)	8.6(3)	7.7(4)	6.8(8)	6(1)	1.5(3)
α_b	11.6(5)	13.0(2)	14.4(3)	15.8(6)	17.1(8)	6.7(3)
α_c	11.4(5)	10.4(2)	9.5(3)	8.5(6)	7.5(9)	8.1(3)
α_α	-5.6(4)	-5.5(2)	-5.3(2)	-5.1(4)	-5.0(7)	-2.0(2)
α_β	-0.4(4)	1.4(2)	3.2(2)	5.0(5)	6.8(7)	-0.6(2)
α_γ	-0.8(3)	0.0(1)	0.8(2)	1.5(3)	2.3(5)	3.2(4)
α_V	32.8(1)	30.9(5)	29.0(6)	27(1)	25(2)	16.4(5)
$\alpha_b(\alpha_{\max})/\alpha_a(\alpha_{\min})$	1.2	1.5	1.9	2.3	2.8	4.5

¹ - [19]

² - μ is an angle between crystallographic axes and eigenvectors (μ_{a1} - between α_a and α_{11} ; μ_{b2} - between α_b and α_{22} and μ_{c3} - between α_c and α_{33})

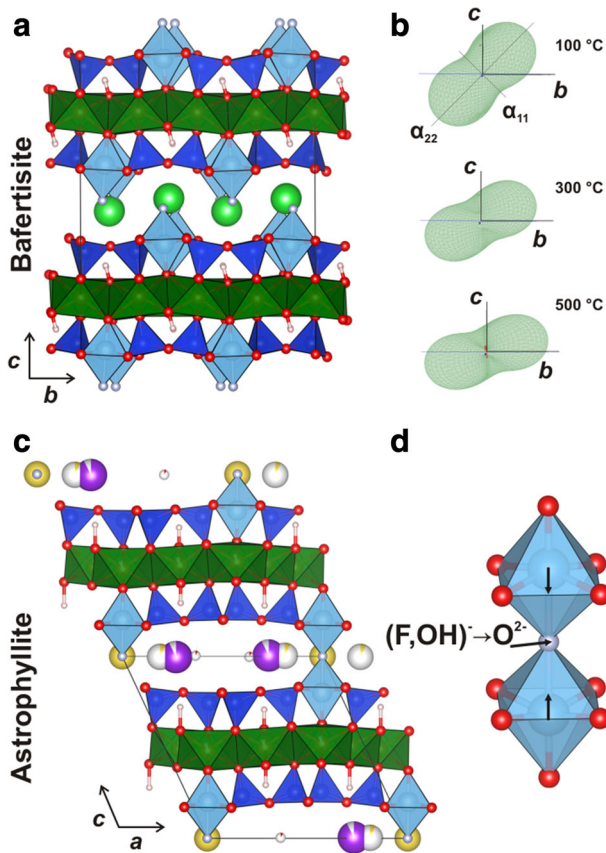


Fig. 6 **a** the crystal structure of bafertisite, **b** figures of thermal expansion of bafertisite; **c** the crystal structure of astrophyllite and **d** linkage of two $Ti\phi_6$ ($\phi = O, OH, F$) octahedra in astrophyllite

$^{\circ}\text{C}$ for astrophyllite) and (iv) evolution of Mössbauer spectra toward the increase of the $\text{Fe}^{3+}/\Sigma\text{Fe}$ ratio after annealing (Table 3). However, the significant difference is in the crystallinity of the high-temperature phase. In astrophyllite, the high-temperature phase has nearly the same intensity of reflections as the initial phase, while the high-temperature phase of bafertisite is characterized by the significant broadening of reflections and the decrease of their intensity (Fig. 2). This indicates that, in the case of bafertisite, the complete iron oxidation does not result in the formation of a stoichiometric (charge-balanced) high-temperature phase as it was observed for astrophyllite. The main condition at which stoichiometric high-temperature (fully oxidized) phase can be obtained is the equality of the positive charge gained during iron oxidation ($\text{Fe}^{2+} \rightarrow \text{Fe}^{3+}$) and the negative charge resulted from deprotonation ($(\text{OH})^{-} \rightarrow \text{O}^{2-}$) that may be accompanied by defluorination ($\text{F}^{-} \rightarrow \text{O}^{2-}$). For example, in the chemical composition of astrophyllite there are usually maximum $5apfu$ of Fe^{2+} (and $2apfu$ refer to Mn, Mg and Na). The oxidation of 5Fe^{2+} in astrophyllite is charge-compensated by: (i) deprotonation of $4(\text{OH})^{-} \rightarrow 4\text{O}^{2-}$ and (ii) defluorination and deprotonation of the X_D^{P} site via the $(\text{F,OH})^{-} \rightarrow \text{O}^{2-}$ substitution (Fig. 6d) [19]. The experimentally determined chemical formula of bafertisite under study is $\text{Ba}_{2.11}(\text{Fe}_{2.70}^{2+}\text{Fe}_{0.17}^{3+}\text{Mn}_{1.09}\text{Zr}_{0.04}\text{Na}_{0.03})(\text{Ti}_{1.96}\text{Nb}_{0.07})(\text{Si}_2\text{O}_7)_2\text{O}_2(\text{OH}_{1.29}\text{O}_{0.65}\text{F}_{0.06})\text{F}_2$. As

Table 3 Selected hyperfine parameters with fitting errors

Sample	Fe	FWHM (mm/s)	IS (mm/s)	QS (mm/s)	A (%)	Fe ³⁺ /ΣFe	χ ²
BaFeTi25	Fe ²⁺	0.458(12)	1.131(11)	2.003(22)	94(2)	0.06(3)	1.16
	Fe ³⁺	0.336(24)	0.585(31)	0.915(46)	6(3)		
BaFeTi600	Fe ²⁺	0.489(12)	1.126(11)	2.025(22)	61(2)	0.39(2)	0.95
	Fe ³⁺	0.772(37)	0.500(43)	1.052(47)	39(2)		

it can be seen from its chemical formula, $1.29(\text{OH})^-$ cannot compensate for the oxidation of 2.70Fe^{2+} . Moreover, defluorination in bafertisite is most probably impossible, due to the absence of the direct linkage of $\text{Ti}\phi_6$ octahedra in comparison to astrophyllite. In astrophyllite, the substitution of F^- by O^{2-} is: (i) equally shared between two $\text{Ti}\phi_6$ octahedra and (ii) expressed in the change of octahedral geometry (shift of Ti to the center of octahedra, which results in the formation of a more regular octahedral coordination) (Fig. 6d). In the crystal structure of bafertisite, $\text{Ti}\phi_6$ octahedra are not linked to each other (Fig. 6a), which weakens the interconnection of adjacent layers and makes the whole structural configuration less rigid. As a result, a stoichiometric high-crystalline fully oxidized modification of bafertisite cannot be obtained. The situation is different with bafertisite studied by Cámara et al. [28], that has the chemical formula $(\text{Ba}_{1.9}\text{Na}_{0.1})(\text{Fe}_{1.8}^{2+}\text{Mn}_{1.6}^{2+}\text{Fe}_{0.4}^{3+}\text{Zr}_{0.1})(\text{Ti}_{1.9}\text{Nb}_{0.1})(\text{Si}_2\text{O}_7)_2\text{O}_2(\text{OH}_{1.8}\text{F}_{0.2})\text{F}_2$, where the Fe^{2+} content matches exactly the OH content. The negative thermal expansion of bafertisite at temperature above 600 °C reported by Cámara et al. [28] agrees well with the process of iron oxidation proposed herein (tacking into account kinetic of heating: 4 °C/min herein and 5 °C/min [28]). In their study [28], authors were able to refine the unit-cell parameters of bafertisite up to $T = 700$ °C. This points out to the general possibility to obtain a high-temperature, fully oxidized modification of bafertisite for different chemical compositions.

Acknowledgments The study was supported through the Russian Science Foundation (grant 17-77-10023). The experiments were carried out using facilities of XRD and Geomodel Resource Centers of St. Petersburg University. We thank Fernando Cámara for valuable comments and Guido Langouche for handling of the manuscript.

References

- Ferraris, G., Bloise, A., Cadoni, M.: *Mesopor. Mater.* **107**, 108–112 (2008)
- Lin, Z., Almeida Paz, F.A., Rocha, J.: Layered titanosilicates. In: Brigatti, M.F., Mottana, A. (eds.) *EMU Notes in Mineralogy*, vol. 11, pp. 123–145 (2011)
- Cámara, F., Sokolova, E., Abdu, Y.A., Pautov, L.A.: *Can. Miner.* **54**, 49–63 (2016)
- Semenov, E.I., Peishan, Z.: *Sci. Rec. (Beijing)* **3**, 652–655 (1959)
- Lykova, I.S., Pekov, I.V., Kononkova, N.N., Shpachenko, A.K.: *Geol. Ore. Dep.* **52**(8), 837–842 (2010)
- Guan, Y.S., Simonov, V.I., Belov, N.V.: *Dokl. Akad. Nauk SSSR.* **149**, 1416–1419 (1963)
- Ferraris, G., Ivaldi, G., Khomyakov, A.P., Soboleva, S.V., Belluso, E., Pavese, A.: *Eur. J. Mineral.* **8**, 241–249 (1996)
- Li, G., Xiong, M., Shi, N., Ma, Z.: *Acta Geol. Sinica.* **85**(5), 1028–1035 (2011)
- Yang, Z., Cressey, G., Welch, M.: *Powder Diffr.* **14**(1), 22–24 (1999)
- Sokolova, E., Cámara, F.: *Miner Mag.* 10.1180/minmag. **081**, 010 (2017)
- Ferraris, G.: *Z. Kristallogr.* **223**, 76–84 (2008)
- Russell, R.L., Guggenheim, S.: *Can Miner.* **37**, 711–729 (1999)

13. Chon, C.-M., Lee, C.-K., Song, Y., Kim, S.A.: *Phys. Chem. Miner.* **33**, 289–299 (2006)
14. Ventruti, G., Zema, M., Scordari, F., Pedrazzi, G.: *Am. Miner.* **93**, 632–643 (2008)
15. Zema, M., Ventruti, G., Lacalamita, M., Scordari, F.: *Am. Miner.* **95**, 1458–1466 (2010)
16. Murad, E., Wagner, U.: *Clay Miner.* **31**, 45–52 (1996)
17. Güttler, B., Niemann, W., Redfern, S.A.T.: *Miner. Mag.* **53**, 591–602 (1989)
18. Veith, J.A., Jackson, M.L.: *Clays Clay Miner.* **22**, 345–353 (1974)
19. Zhitova, E.S., Krivovichev, S.V., Hawthorne, F.C., Krzhizhanovskaya, M.G., Zolotarev, A.A., Abdu, Ya.A., Yakovenchuk, V.N., Pakhomovsky, Ya.A., Goncharov, A.G.: *Phys. Chem. Miner.* <https://doi.org/10.1007/s00269-017-0886-1> (in press)
20. Piilonen, P.C., LaLonde, A.E., McDonald, A.M., Gault, R.A., Larsen, A.O.: *Can Miner.* **41**, 1–26 (2003)
21. Sokolova, E., Cámara, F., Hawthorne, F.C., Cirotti, M.: *Miner. Mag.* **81**, 143–150 (2017)
22. Bruker, A.X.S.: Karlsruhe, Germany (2009)
23. Belousov, R., Filatov, S.: *Glass Phys. Chem.* **33**(3), 271–275 (2007)
24. Bubnova, R.S., Firsova, V.A., Filatov, S.K.: *Glass Phys. Chem.* **39**(3), 347–350 (2013)
25. Langreiter, T., Kahlenberg, V.: Institute of mineralogy and petrography. University of Innsbruck, Austria (2014)
26. Shino, I., Li, Z.: *Hyperfine Interact.* **116**, 189–196 (1998)
27. Wu, G., Wang, Y., Zhang, S., Ding, H.: *Acta Petrologica Mineralogica et Analytica* **1**(1), 23–28 (1982). in Chinese with English abstract
28. Cámara, F., Arletti, R., Sokolova, E., Hawthorne, H.: IMA 2014 Conference of Proceedings, p. 346 (2014)